White Rose Research Online

eprints@whiterose.ac.uk
https://eprints.whiterose.ac.uk
Universities of Leeds, Sheffield and York

Deposited via The University of Sheffield.

White Rose Research Online URL for this paper:
https://eprints.whiterose.ac.uk/id/eprint/241819/

Version: Accepted Version

Article:

Shackleton, H.R., Skipper, W. and Lewis, R. (2026) New observations on the effect of roughness and third-body layers on friction at the wheel/rail interface. Wear, 593. 206619. ISSN: 0043-1648

https://doi.org/10.1016/j.wear.2026.206619

© 2026 The Authors. Except as otherwise noted, this author-accepted version of a journal article published in Wear is made available via the University of Sheffield Research Publications and Copyright Policy under the terms of the Creative Commons Attribution 4.0 International License (CC-BY 4.0), which permits unrestricted use, distribution and reproduction in any medium, provided the original work is properly cited. To view a copy of this licence, visit http://creativecommons.org/licenses/by/4.0/

Reuse
This article is distributed under the terms of the Creative Commons Attribution (CC BY) licence. This licence allows you to distribute, remix, tweak, and build upon the work, even commercially, as long as you credit the authors for the original work. More information and the full terms of the licence here: https://creativecommons.org/licenses/

Takedown
If you consider content in White Rose Research Online to be in breach of UK law, please notify us by emailing eprints@whiterose.ac.uk including the URL of the record and the reason for the withdrawal request.

UNIVERSITY OF LEEDS University of Sheffield UNIVERSITY of York

New Observations on the Effect of Roughness and Third-Body Layers on Friction at the Wheel/Rail Interface

H.R. Shackleton, W. Skipper, R. Lewis*

The University of Sheffield, Department of Mechanical Engineering, Mappin St, Sheffield, S1 3JD.

* corresponding author: roger.lewis@sheffield.ac.uk

Abstract

Friction at the wheel/rail interface is critical for safe and efficient operation of railways. Low friction due to leaf layers or the "wet-rail" phenomenon can cause safety issues and delays. High friction can lead to increased energy consumption, accelerated wheel and rail damage, and plays a role in wheel climb derailments. These can occur after or rail grinding operations which increase roughness of wheel and rail surfaces thereby increasing the lateral forces present at the interface. Although these rough surfaces wear in relatively quickly, there is a period where the risk of an accident is raised.

Rail roughness effects on friction have not been extensively studied. One reason for this is the difficulty in measuring roughness evolution.

In this work novel friction measurements were taken using a high-pressure torsion approach. Wheel and rail specimens were used and different initial rail roughness'. Friction was recorded cycle by cycle along, uniquely, with roughness. Dry tests were run with tests using third body layers. New relationships between friction and roughness and unique friction datasets have been determined that could now be integrated into multi-body dynamics simulations, via a creep force model, designed to predict wheel/rail interface behaviour in similar rail roughness conditions.

Keywords: Roughness, Friction, Traction Coefficient, Wear, Wheel, Rail, Third-Body Layers

1. Introduction

Globally, travelling by rail is one of the most popular modes of transport thanks to its low environmental impact, low cost and short journey times when compared to other transport methods. Whilst rail transport's popularity is not in question, there are a great many challenges that must be overcome to provide a safe and reliable railway network. One such challenge is obtaining the correct levels of traction/adhesion at the wheel/rail interface. Where the traction/adhesion is defined as the tangential friction force between the wheel and the rail. Low adhesion, mainly occurring during Autumn when leaf layers can reduce friction levels to around 0.05 [1, 2], is estimated to cost the UK rail network £350m per annum [3]. These less-than-ideal conditions result in longer braking and acceleration distances which in turn result in station overshoots and timetable delays. Traction/adhesion coefficients of no less than 0.15 are required for a safe, efficient railway [4]. If adhesion is too high, however, wheels and rails are subjected to high shear stresses which result in excessive wear [5-6], higher energy consumption [7] and there is a higher risk of wheel climb derailments [8-9]. Many aspects alter adhesion, from external contaminants such as water or leaves to the interfacial material properties and their condition. This makes predicting and correcting substandard adhesion conditions challenging. Traction/adhesion is quantified by the traction/adhesion coefficient μ (the ratio of tangential to normal pressure at the interface). Greater traction coefficients mean higher friction at the interface, so by improving the fundamental understanding of the wheel/rail interface it is hoped that countermeasures can be introduced to mitigate adverse adhesion issues.

The roughness of wheels and rails is not static, but evolves over time. Most notably when they are reprofiled during wheel turning and rail grinding operations [10]. The high resultant roughness these processes produce is cause for concern, as they are now thought to increase lateral flange forces and the likelihood of derailment through a process known as wheel climb [8-9]. Frictional changes due to roughness have not been extensively studied, in part due to the difficulty in measuring the evolution of roughness during a test. Some work has been performed however, most notably the work by Fukagai et al., whereby roughness was measured during dry contact multi-cycle high pressure torsion (HPT) tests, however, the roughness was not measured frequently nor did this work cover the presence of third-body layers (3BLs) [11]. In addition, Chen et al. used twin disc and roller rig testing to demonstrate that both elevated temperature and surface roughness act to increase the traction coefficient at least for wet contacts [12, 13]. Both these bodies of work used line roughness, not areal roughness, to evaluate the surfaces condition.

The advantage of the HPT test approach is that the test specimens are flat and therefore adding roughness can be done in a representative way more easily and applying third-body materials is easier. Also the tests can be run one cycle at a time with measurements in between to assess surface changes. One cycle can also provide enough data to create, within an appropriate creep force model, a creep curve giving full detail of the slip/friction relationship for a wheel/rail interface with the particular conditions present. In previous work an approach has been developed where HPT data has been used to parameterise the "Extended Creep Force" model allowing full-scale predictions to be carried. This has been validated for the application of water-based top-of-rail friction modifiers (used to give intermediate levels of friction in the wheel/rail interface) [14, 15] and sand application for traction enhancement [16].

A gap is clearly evident in the knowledge concerning roughness evolution, particularly at a cycle-by-cycle resolution and with the complexity of a third-body layer present. The aim of this work was therefore to evaluate the impact of rail roughness on wheel/rail interface friction and how both evolve cycle-by-cycle. This included the impact of third body layers. Leaf layers known to cause low adhesion were created and evaluated along with grease, used in curves to reduce friction and water, a naturally occurring rail head contaminant. The interplay between roughness and friction evolution has not been well studied for dry contacts and not at all with the inclusion of different materials within the interface. Roughness scenarios considered were a "run-in" rail, where the running band is typically in the range of 0.5-1μm Ra and a freshly ground rail, either from a preventive process designed to return the rail to its optimum profile, or a corrective process for damage removal where roughness' can reach up to 10μm. The high pressure torsion test approach was selected as this can provide a means, in conjunction with a creep force model, to provide predicted creep curves for a full-scale wheel/rail interface that can then be used in multi-body dynamics simulations to assess train performance where these interface conditions have occurred or in train braking simulations, such as those from the LABRADOR model [17].

2. Roughness Theory

Rail grinding is a process performed on the railhead that returns it to the correct rail profile. The high resultant roughness this process produces can be seen in Figure 1(a).

(a)

(b)

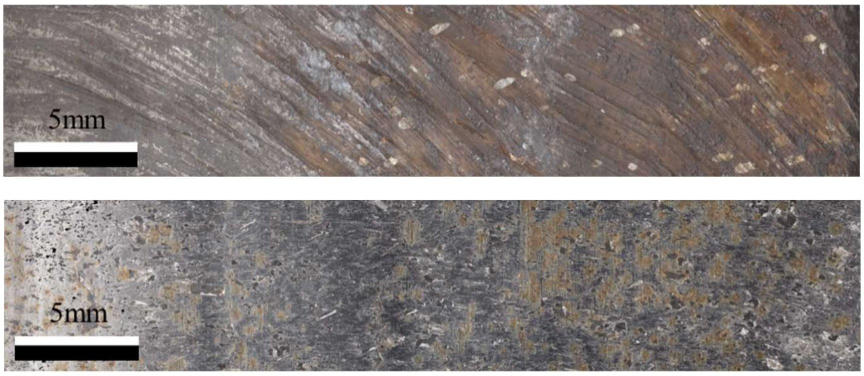

Figure 1. (a) Ground and (b) run-in railheads

After the rail grinding process, the hardened plastically deformed layer on the railhead is removed to make way for a softer and rougher machined surface. The railhead is then run-in whereby the surface asperities created by the grinding process are plastically deformed resulting in a surface that has been hardened and is lower in roughness (see Figure 1(b)). This process was focused on to study the evolution of roughness at the wheel/rail interface, where roughness generally starts from around 8-10µm and reduces to around 1-2µm when run-in [10]. A cyclical HPT test approach was used to simulate the "passing" of wheels whilst allowing the intermittent measurement of roughness.

There are many parameters used to describe surface topography, these include skewness, kurtosis and roughness. This work only covers roughness, however, it would be wrong to suggest that these other surface properties do not affect the way surfaces interact with one another. There are many ways to define roughness, R_q provides a quick easily computable line roughness value that is widely used. S_q is a measure of the areal roughness and is calculated using Equation 1, where z is a function of the asperity heights in x and y directions over area A. Whilst computationally more difficult than R_q, it gives a more comprehensive picture of a surfaces roughness by considering directionality:

$$S_q = \sqrt{\frac{1}{A}\iint z^2(x,y)dxdy} \qquad (1)$$

When two surfaces come into contact the surface asperities plastically deform as locally their contact generates very high contact stresses and the surfaces begin to conform to one another. Since both surfaces are changing it can be useful to unify the two separate roughness' as a single system roughness. By defining this composite roughness $S_{q\sigma}$, lower (S_{q1}) and upper (S_{q2}) specimen roughness can be combined into a single value (see Equation 2):

$$S_{q\sigma} = \sqrt{S_{q1}^2 + S_{q2}^2} \qquad (2)$$

Combining the component roughness' in this way gives greater prevalence to specimens with high roughness than simply summing the component parts. This better represents surface interactions whereby large asperities penetrate the other surface.

3. Method

The specimen manufacture and testing procedure is discussed here as well as how the roughness and friction measurements were achieved.

3.1 Specimens

Upper wheel and lower rail specimens were manufactured from wheel and rail material (ER8 and R260 respectively). The material properties can be seen in Table 1.

Material	*Yield Strength (MPa)*	*Tensile Strength (MPa)*	*Hardness (HB)*
R260	420	880	260-300
ER8	590	940	230-260

Table 1. Approximate specimen material properties [18-19]

The specimen geometries when brought together produced a flat-on-flat annular contact. Various machining processes were attempted on the interfaces to provide S_q values in the same region as ground rail. The lower rail specimens were fly cut with a 0.8mm pitch to produce the high initial roughness conditions (9-10µm) and ground to produce low initial roughness conditions (1-2µm). The upper, wheel specimens were ground to produce low initial roughness conditions (1-2µm) for all tests.

3.2 High Pressure Torsion (HPT) Test Method

The HPT test is an emerging tribological test that has advantages over twin-disc and pin-on-disc testing as 3BLs can be applied more easily and initial roughness can be machined onto to the specimens with relative ease [14, 15, 20-22]. Additionally, only one cycle is required to produce shear stress data and traction/adhesion coefficients. These traction/adhesion coefficients can then be compared to surface roughness, which can be measured cycle by cycle. A schematic of the HPT machine can be seen in Figure 2.

The HPT test involves the use of two flat specimens, the lower rail (R260) specimen and the upper wheel (ER8) specimen (1 and 2 respectively) that are pressed together with a certain force and then twisted through a predefined rotation angle. The contact patch made is that of an annulus. These specimens are attached to the rig with specimen holders (3). Specimens are kept separate initially and then brought together during testing. Normal pressure is applied with an axial hydraulic actuator (6) and the rotation is applied using a rotational hydraulic actuator (5). These actuators are pressurised using a hydraulic ring main (10) to around 25 MPa. Servo valves control the flow of hydraulic fluid to these actuators which are controlled with an electrical control unit (8). A Linear Variable Differential Transformer (LVDT) and load cell (7) send axial displacement and load information to the control unit. Similarly, a Rotary Variable Differential Transformer (RVDT) and load cell (6) send rotational displacement and load information to the control unit. The control unit is equipped with two channels (axial and rotational) thereby permitting the control of test specimens in both these directions. A hydraulic crosshead (9) allows specimens of 500-2000 mm in length to be tested.

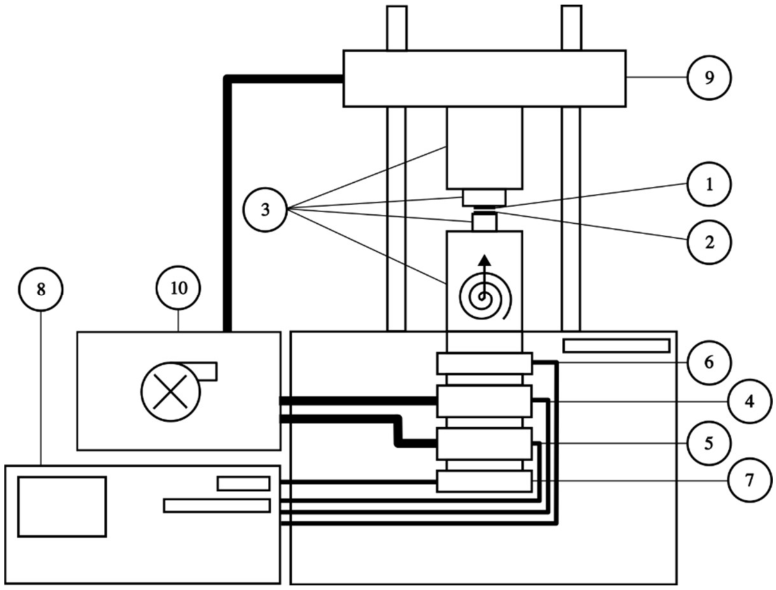

Figure 2. HPT rig schematic [14]

The operational limits of the HPT machine are shown in Table 2. The HPT rig can be seen in Figure 3 as well as the specimen assembly. Specimens can be separated and removed between testing cycles to apply 3BLs and take replicas of the surfaces from which roughness measurements can be taken.

Operation	***Operation Limit***
Axial Load	+/- 400kN
Axial Displacement	+/- 25mm
Torque	+/- 1000Nm
Torsional Displacement	+/- 40 degrees

Table 2. HPT operational limits

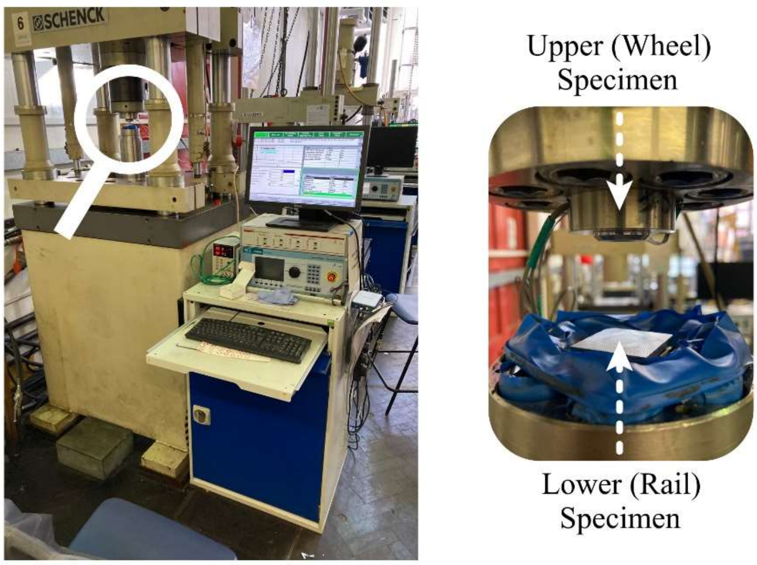

Figure 3. HPT rig and specimens

Figure 4 shows a typical 600MPa test procedure. Axial compression is applied, tangential pressure is built up and the specimen rotates through a predefined sweep length at a certain sweep rate. Upon the initial application of tangential pressure the contact acts elastically, i.e. tangential pressure increases linearly with rotation position. As the tangential pressure increases, this eventually results in the plastic deformation of asperity level contacts and the tangential pressure reaches a somewhat static value until the torque is released upon completion of the cycle. Whilst rotation position is programmed to increase linearly through the test, the result of plasticity at asperity contacts (i.e. localised stick-slip) results in some variation away from this idealised situation and also results in variations in tangential pressure. A more in-depth explanation of these phenomena is given in [16, 23].

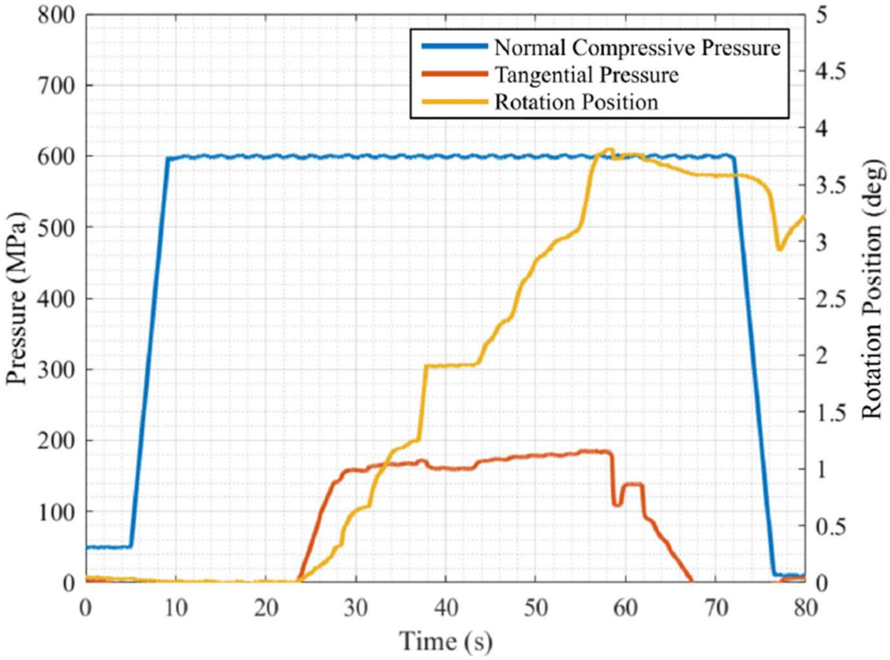

Figure 4. Typical HPT test procedure

The tension-compression-torsion load cell on the HPT rig was able to measure the force being applied through the HPT. However, to convert this force into pressure, the contact area between the two specimens must be calculated. This was achieved with pressure sensitive film that creates a measurable annulus. This stage was also conducted to check the alignment of the two specimens to ensure an even load distribution over the entire annulus. The alignment check was performed at 150MPa at the −40°, 0° and 40° locations.

Whilst creep stresses are assumed to be uniform across the annular contact patch, at higher radii these same creep stresses have a greater contribution to the torque. This means the midpoint between the inner and outer radius cannot be used to calculate the creep stress from the measured torque. Therefore, in addition to the area calculation, the effective radius of friction (ERF) must be calculated to define a point through which torque acts. Figure 5 and Equation 3 and show the effective radius of friction and how it is calculated where r is the inner radius and R is the outer radius [14].

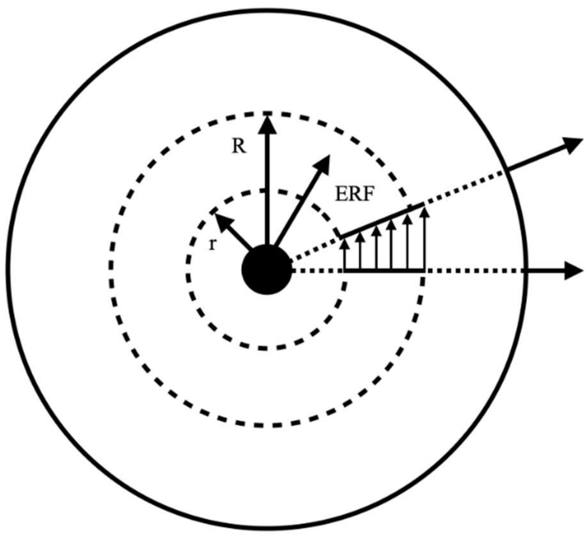

Figure 5. Effective radius of friction (ERF)

$$ERF = \frac{2}{3}\left(\frac{R^3-r^3}{R^2-r^2}\right) \quad (3)$$

Inner and outer radii were measured using calipers. The ERF was calculated for each test as specimen geometry varied due to manufacturing tolerances. Specimens were reused which required regrinding to achieve the desired initial roughness. When this occurred, the annular area increased due to the chamfered nature of the geometry and so the ERF was recalculated, and the HPT test parameters updated. Calculation of the ERF enables the measured torque to be converted into tangential load. The ratio of the tangential and normal loads (*T* and *N*) is the traction coefficient (see Equation 4).

$$Traction\ Coefficient = \frac{T}{N} \quad (4)$$

3.2.1 HPT Script Design

As with most tribological tests the testing process was automated using a script. Test parameters were inputted into this script which then ran using these parameters. A PID controller used these parameters to command the servo valves to move the HPT in both axial and rotational directions at the desired speed and force. A list of test parameters is shown below:

- Number of Cycles
- Pressure
- Contact Area
- ERF
- Sweep Length
- Sweep Rate
- Step Rotation

Temperature and humidity were measured but not controlled. Typical laboratory temperature during test was 20--30°C and humidity 40-50%. Although these parameters are known to have an impact on frictional behaviour; the control of temperature and humidity was out of the scope of this work. Some parameters were defined by the specimen such as the contact area and ERF and some were inputted by the operator. These include contact pressure, number of cycles, sweep rate and sweep length. In addition to these, there were certain aspects of the testing process that were specified in order to tailor the tests to the operator's needs. Figure 6 shows the test sweeps of test cycles one and two. By overlapping tests many repeats could be performed within the HPT rotational limits outlined in Table 2. However, once the majority of the contact had reached a limiting creep stress, this method often caused the interface to suddenly slip releasing some of the elastic energy that had been built up. This release of elastic energy decreased the creep stress required to stop the slippage and the process repeated itself as a feedback loop [14]. To perform 20 cycles and avoid this behaviour, ten separated cycles were performed then the specimens were rotated back to the start and the process was repeated. This process mitigated undesirable slipping events whilst allowing 20 cycles to be performed.

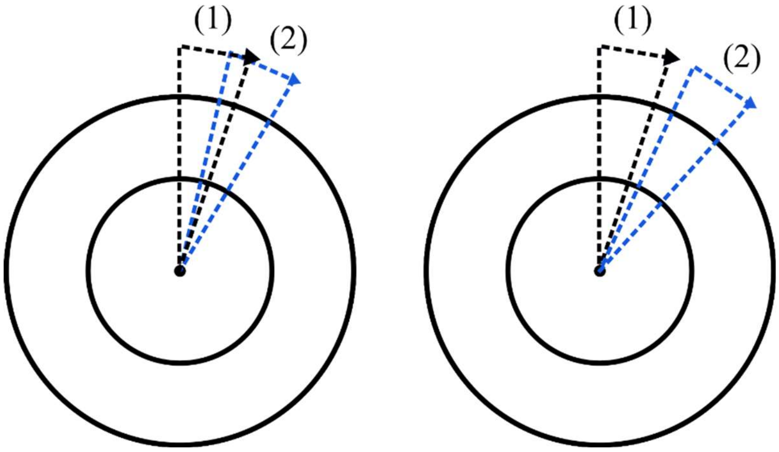

Figure 6. Schematic showing overlapped and separate test sweeps

The sweep distance acts at the ERF, which for the HPT tests is around 7.3mm. The sweep length must be large enough to ensure all the frictional behaviour is obtained for use in model parameterisation. Evans et al. concluded that a sweep length of 0.4mm ensured the whole interface had entered the sliding regime [14]. This translates to a sweep angle of around 3 degrees. To ensure that the cycles do not overlap a step rotation of around 2 degrees is added between each cycle.

Table 3 shows the rotation start and end points for the first ten cycles. The second ten cycles use the same start and end points as the rotation range was not sufficient to host 20 cycles. Note the two-degree discrepancy between rotation end points and start points. This is the step rotation shown in Figure 6 that reduced undesirable slip. Between cycles the HPT specimens are separated to allow for specimen cleaning, roughness measurements and for 3BL application.

Cycle	*Rotation Start (°)*	*Rotation End (°)*
1	-30	-27
2	-25	-22
3	-20	-17
4	-15	-12
5	-10	-7
6	-5	-2
7	0	3
8	5	8

9	10	13
10	15	18

Table 3. HPT cycle rotation index

The final parameter was the sweep rate. Slower sweep rates (≈ 0.02 deg/s) result in very repeatable results but extend the test time. Higher sweep rates (≈ 1 deg/s) result in fast tests but introduce frictional heat that manifests as a rising creep stress as sliding progresses [14]. A sweep rate of 0.1 deg/s was used for all HPT tests. The full list of HPT test parameters can be seen in Table 4.

Parameter	*Value*	*Units*
Number of Cycles	20	
Pressures	600, 750, 900	MPa
Contact Area	Measured	mm^2
3BL	Dry, Water, Grease, Leaves	
Surface Roughness (S_q)	Rough (7-8), Smooth (1-2)	µm
ERF	Measured	mm
Sweep Length	≈ 3	°
Sweep Rate	0.1	°/s
Step Rotation	≈ 2	°
Temperature	Measured	°C
Humidity	Measured	%

Table 4. HPT test parameters

Contact pressures selected are typical of those seen in the wheel tread/rail head contact [24]. Roughness values were chosen to represent and run-in rail and a freshly ground rail (via a grinding train).

3.3 3BL Application Method

Alongside dry tests, three 3BLs were studied to better understand how roughness affects these layers and their influence on roughness evolution. The 3BLs are listed below:

- Distilled Water
- Sycamore Leaves
- Grease

Each required slightly different application procedures. For dry tests the specimens were cleaned with acetone before testing and after each cycle.

3.3.1 Distilled Water

Water occurs naturally on the railhead. Low amounts of water such as when it has just started to rain or early in the morning in the form of dew cause low adhesion [25]. 20µL of distilled water was applied to the lower specimen contact area with a pipet before testing and after each cycle. Specimens were cleaned with acetone before testing and after each cycle.

3.3.2 Sycamore Leaves

Leaves are a major industry issue as they cause low adhesion when they are compressed to form a leaf layer. Sycamore, Horse Chestnut, Sweet Chestnut, Ash, Poplar and Common

Lime have all been identified as "problem leaves" by the Adhesion Working Group (AWG), meaning their presence on the railhead results in ultra-low adhesion conditions ($\mu<0.1$) that negatively impact safe railway operation [3]. 0.025g of dried sycamore leaf powder was applied to the lower specimen contact area before the test. Hydration of 20µL occurred to the lower specimen contact area before the test and after cycles 1, 4, 7, 10, 13, and 17. The leaf layer was removed after the test using an ultrasonic water bath to measure the final roughness.

3.3.3 Grease

Grease is applied to the rail gauge corner to reduce the interfacial friction conditions and reduce wear. The grease used was a common oil-based grease. 0.012g was applied to the lower specimen contact area before the test and after cycles 5, 10 and 15. The specimens were cleaned with acetone after these cycles to measure the roughness.

3.4 Roughness Measurement Method

Overall, the parameters that can be used to define surface topography number over 50. So many defining parameters makes studying roughness difficult. A single combined roughness parameter σ was used to study the evolution of interfacial surface roughness. The measurement of roughness evolution was measured using surface replicas. Replication compound was applied to the upper and lower specimens at various intervals during testing. The frequency of replication depended on the test. Where surfaces were dry or the 3BL could easily be removed, replication occurred often, but when the 3BL was difficult to remove replication occurred less often (see Table 5).

Test	*Replication Occurred After Cycles…*
Dry	0,1,2,3,4,6,8,10,15,20
Water	0,1,2,3,4,6,8,10,15,20
Grease	0,5,10,15,20
Leaves	0,20

Table 5. Replication index

Surface scans were taken from these replicas using a non-contact surface profiler (InfiniteFocus, Alicona); the scan locations relative to the specimens are shown in Figure 7. Three surface scans were taken per replica. Each scan provided a roughness value which were then averaged to denote the global roughness. Higher deviations from this average indicated localised wear.

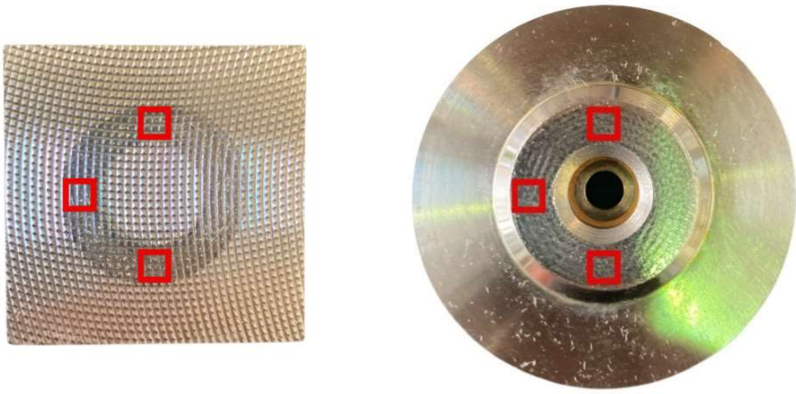

Figure 7. Scan locations on the lower (left) and upper (right) specimens

Surfaces exhibit two kinds of topography, small-scale variations (roughness) and large-scale variations (waviness). These two characteristics are often studied separately. To do this high and low pass filters are applied to separate small-scale and large-scale surface elements. By applying a cut-off wavelength, λ_C, to surface roughness scans, low frequency waviness can be filtered out, as seen in Figure 8. The filter removes large variations in surface height creating a flat plain from which surface texture protrudes and recesses. Common λ_C values include 0.08mm, 0.25mm, 0.8mm, 2.5mm and 8mm depending on the roughness of the surface [26].

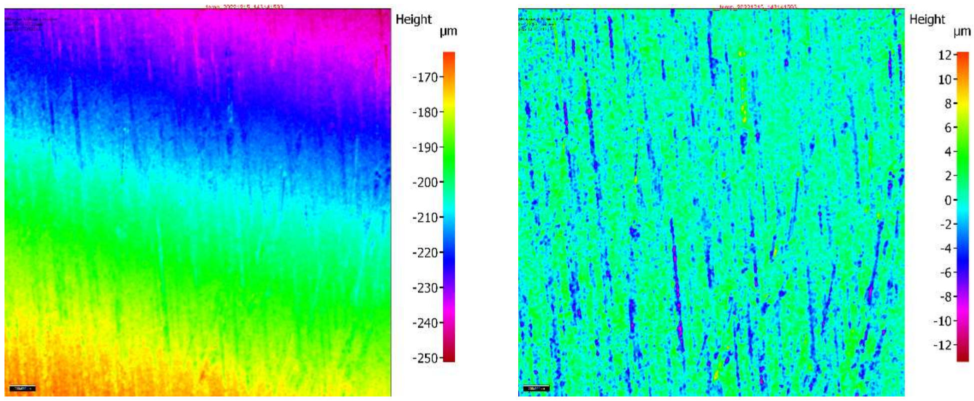

Figure 8. Effect of Gaussian filters on an Alicona surface scan (Left: Filter Off. Right: Filter On)

Scan size was set to 3x3mm which was the largest area size that could be reasonably and consistently measured from the contacting annulus. Measurement length, L_C = 3mm and cut-off wavelength, λ_C = 0.8mm. It can be seen from Figure 8 that this cut-off wavelength produced a good representation of roughness, reducing waviness whilst not destroying surface texture. This measurement area and cut-off wavelength were then applied to every other roughness measurement to ensure a consistent measurement approach was being applied. It was assumed that the average roughness of the three 3x3mm measurement squares was representative of the roughness of the full contact.

4. Results and Discussion

The evolution of roughness for both high and low initial roughness' is reported and discussed, as is its relation to the traction coefficient and what this means for wheel/rail interfacial conditions.

4.1 Roughness

Two initial roughness' were studied, high initial roughness (HIR) and low initial roughness (LIR) which relate to the relative roughness' of the lower (rail) specimens. Figure 9 shows the separate roughness evolutions for lower (rough) and upper (smooth) HPT specimens for the dry HIR tests. The two separate roughness' were combined using Equation 2 to produce the combined roughness shown in Figure 10. Initial roughness' were applied using fly cutting (rough) and grinding (smooth) procedures. Aside from the small amounts of work hardening that these processes induce no prior run-in was performed on the specimens as this would alter the initial roughness. The smoother ground surface was penetrated by the rougher fly cut surface (see Figure 9(c)) which resulted in roughness transfer from the lower to the upper specimens which collectively decreased with increased cycles. The rate at which the roughness changes is altered due to the work hardening and conformation of the two materials as they are pressed together and rotated against one another. Whilst only 20 cycles were performed in these tests, similar work by Lewis et al. using a twin disc machine has shown roughness progressions of around 9-10µm to 1-2µm although this was performed for many more cycles [27]. The field measurements produced by Lundmark et al. also show this level of roughness progression following reprofiling events in the real world [10]. Given a sufficient number of cycles the roughness of the two opposing surfaces in Figure 9 are expected to progress to a common roughness similar to those found in these two studies.

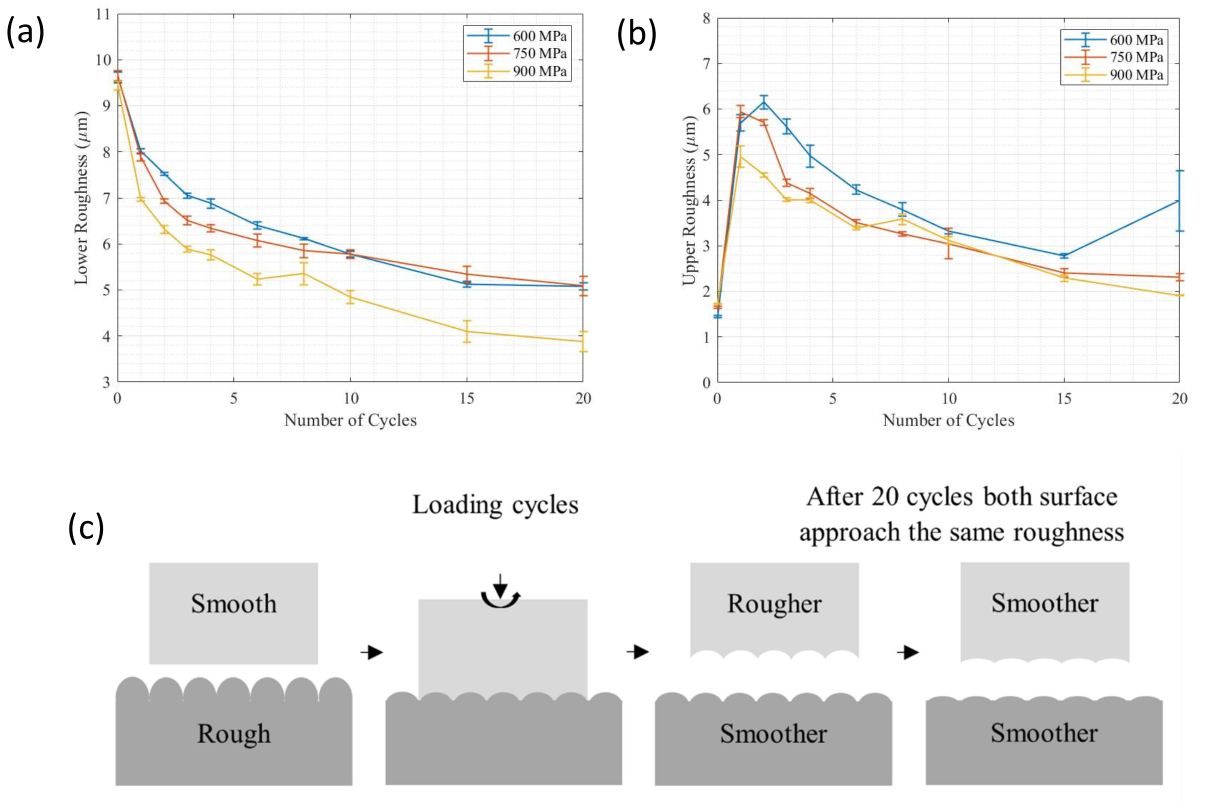

Figure 9. HIR dry test: (a) lower surface roughness (S_{q1}); (b) upper surface roughness (S_{q2}) and (c) associated mechanism schematic

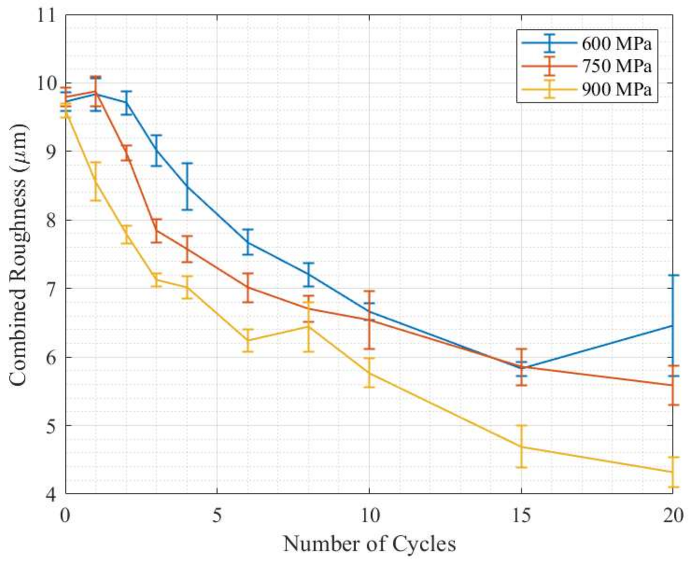

Figure 10. HIR dry test combined roughness ($S_{q\sigma}$) evolution

4.1.1 Roughness - High Initial Roughness (HIR)

HIR tests began at a combined roughness of around 9-10µm. Combined roughness shows a general decrease for dry, water, grease, and leaf tests, as shown in Figure 11. Greater pressures result in larger roughness decreases. This is in agreement with previous HIR tests performed by Fukagai et al. [11].

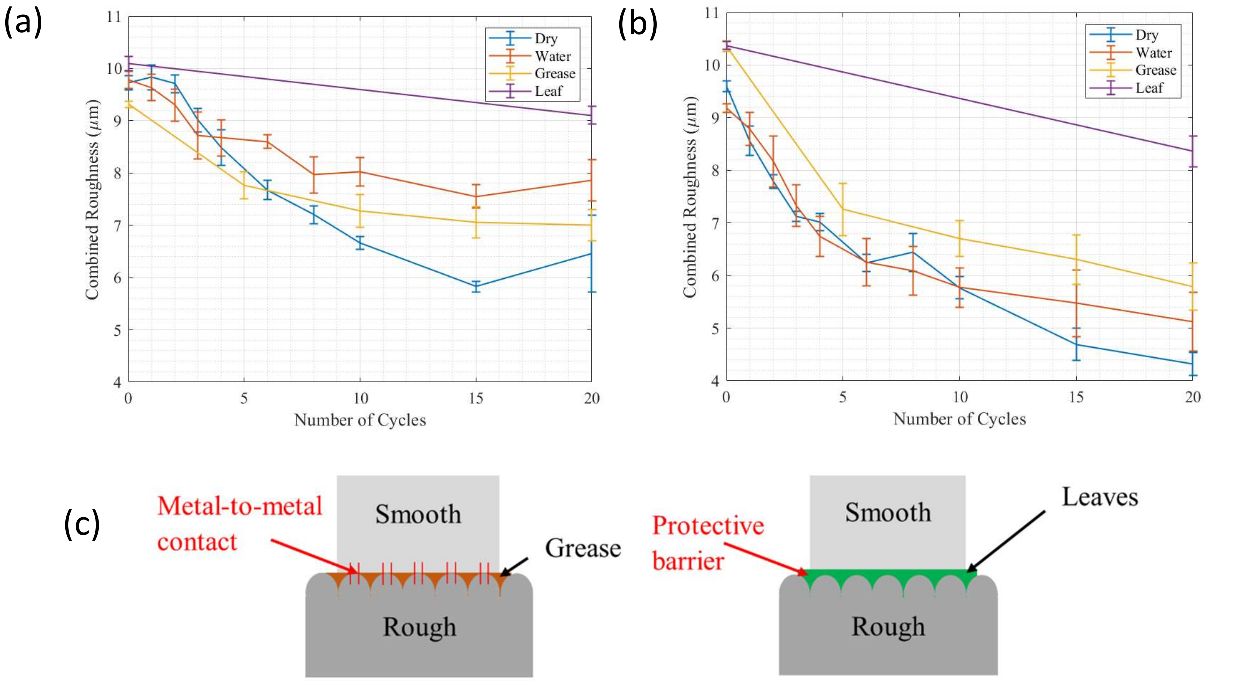

Figure 11. HIR 3BL tests combined roughness ($S_{q\sigma}$) evolution: (a) 600 MPa; (b) 900 MPa and (a) associated mechanism schematics

The specimens were reused by grinding back the worn surfaces and applying a new surface roughness before each new test. No manufacturing process is perfect and slight variations in surface texture were introduced due to the manufacturing uncertainties. The operator, feed rate, depth of cut and the sharpness of the tool all alter the finished surface. Pairing this with variation in the measurement process meant that the initial roughness varied from specimen to specimen by up to 1µm.

Figure 12 shows the lower HIR specimens after 20 cycles. The presence of leaves protected the surface resulting in only small roughness reductions. Dry, water and grease specimens were visually similar after 20 cycles with small amounts of wear being incurred on the dry specimen. However, the water and grease did provide some protection as indicated in their lower roughness reduction. It is perhaps surprising that the grease did not offer more protection; it is possible that the roughness may have provided a space for grease to accumulate so not all of it is in the interface allowing metal-to-metal contact as shown in the mechanism schematic in Figure 11(c).

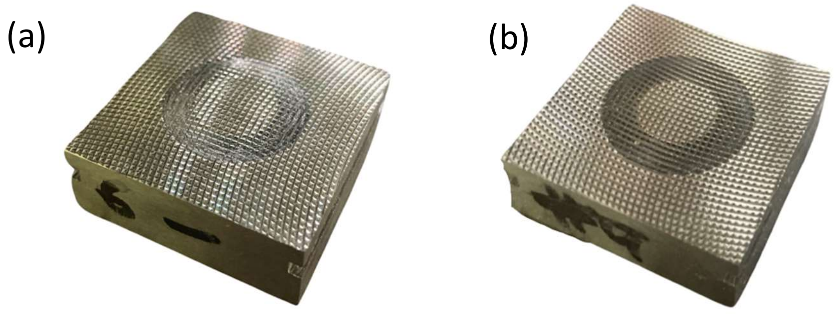

Dry – HIR – 900 MPa – 20 cycles   Water – HIR – 900 MPa – 20 cycles

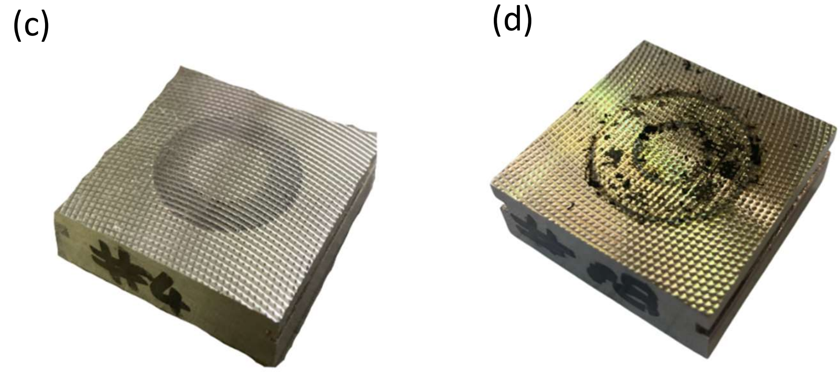

Grease – HIR – 900 MPa – 20 cycles   Leaves – HIR – 900 MPa – 20 cycles

Figure 12. HIR 900 MPa 3BL tests final lower roughness: (a) dry; (b) water; (c) grease; (d) leaves)

4.1.2 Roughness - Low Initial Roughness (LIR)

Low initial roughness tests began at a combined roughness of around 2-3μm (see Figure 13). During dry tests adhesive wear occurred which led to the increased combined roughness seen. Wear debris was created which potentially acted as a solid lubricant increasing the likelihood of larger slip events. The production of this debris promoted third-body abrasive wear which further increases surface wear. Debris was removed during inter-cycle cleaning and replication thereby reducing this effect. Water tests were susceptible to large slip events as the amounts of water were not sufficient to fully lubricate the surfaces, but were sufficient to permit oxide build up (see Figure 14). Small amounts of water alongside iron oxides are known to form a paste that lowers adhesion [28]. Surfaces are initially protected by the oxides, but are then cleared during slip and inter-cycle cleaning. When the interfacial shear stress exceeds the shear strength of these oxides slip occurs as the oxides break away. The nature of this stress build up and subsequent release may have increased the likelihood of these larger more damaging slip events [21]. These are not typical of actual wheel and rail surfaces. Slip due to "wet-rail" would not happen often and subsequent wheel cycles would remove it anyway before it could be observed. Grease and leaves effectively lubricated the interface resulting in very little roughness change over the entirety of the tests. The presence of grease resulted in a mild, controlled wear process that reduced system roughness slightly by polishing the surfaces. Roughness for most tests was assumed to be constant around the annular contact, however for tests that incurred such large amounts of random localized wear this assumption was no longer reasonable.

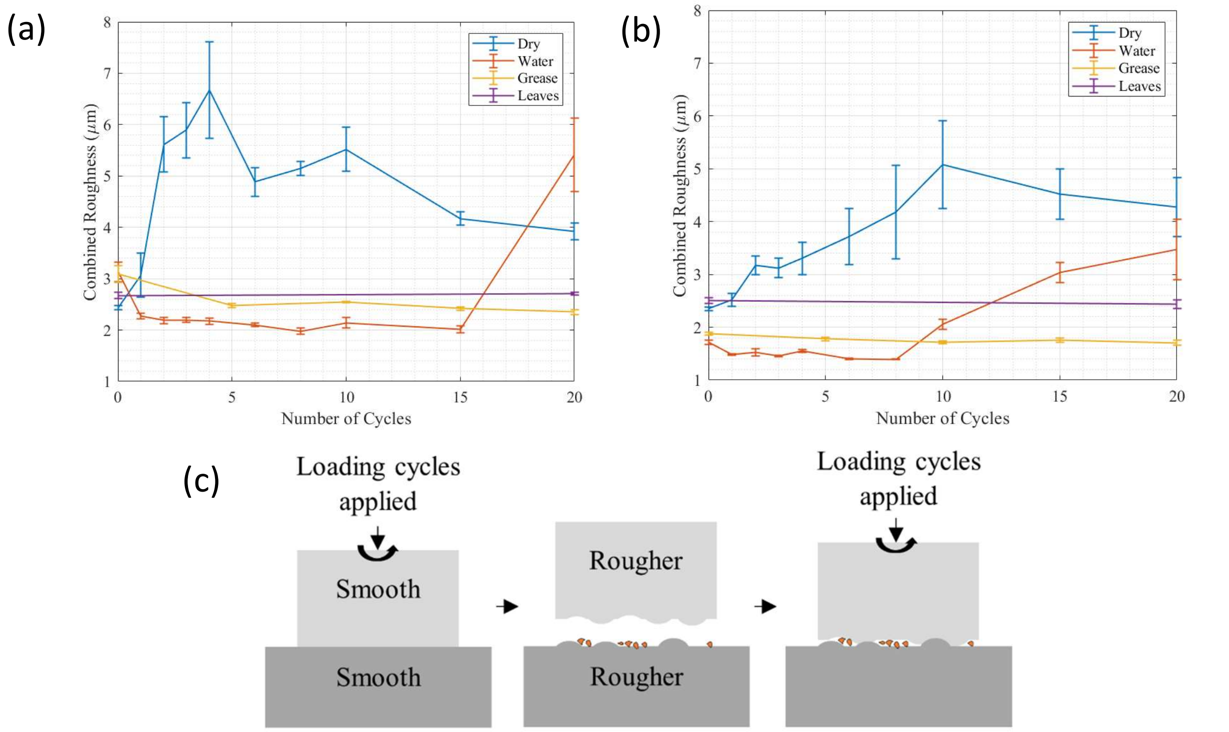

Figure 13. LIR 3BL tests combined roughness ($S_{q\sigma}$) evolution: (a) 600 MPa; (b) 900 MPa and (c) associated mechanism schematic

Figure 14 shows an Alicona scan of a replica indicating the presence of oxides as well as evidence of adhesion and abrasion. These oxides and debris were detached from the metal surface when the replica was removed. The formation of an oxide paste may have lowered adhesion and caused portions of the interface to break free. This debris was then introduced to the interface causing additional third-body wear. During cleaning between cycles these particles were mostly removed. This was essential to measure the surface roughness, but it is expected that the wear would have been greater if these debris particles were left in place.

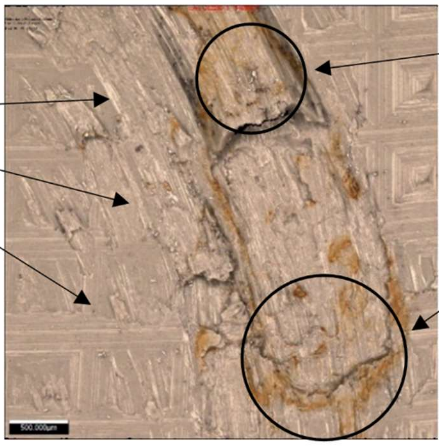

Figure 14. Wear induced by oxide layers on water tests

4.2 Friction

Friction is quantified by the traction coefficient, the ratio of tangential to normal load (see Equation 4). During running in the surface topography changed which in turn changed the way the two surfaces interacted. This indicates that during the run-in phase a system's friction is dependent on the surface roughness [29]. To compare the traction coefficients of different tests an average was taken of the traction coefficient during the middle 20 seconds of the rotation phase of the test.

4.2.1 Friction - High Initial Roughness (HIR)

Figure 15 shows the traction coefficient evolution for the HIR tests. Contact pressure had an impact on the dry tests where at higher pressure, friction was lower in line with previous tests [27]. It had negligible effect on the traction coefficients for the most tests where there were third body layers added, however, some variation was observed. Higher pressures were able to run-in the surfaces and reduce the surface roughness more effectively than lower pressures (as shown in Figures 9 and 10). Friction force is made up of two components, the adhesion force, and the ploughing force. The adhesion force depends on the real area of the contact made by the interacting asperities whereas the ploughing force depends on the hardness of the two interacting materials, specifically the force required to force the harder materials asperities into the softer material (HIR ploughing can be seen in Figure 16). For run-in surfaces, friction is dominated by the adhesion component, however, during running-in, the ploughing component is relevant which depends on the surface roughness.

As shown in Figure 15, leaves produced extremely low traction coefficients ($\mu < 0.1$) This is in line with previous HPT tests with leaves and leaf layers [14]. Friction rose with increased cycles as the leaf layer was degraded and more metal-to-metal contact occurred. The presence of water lubricated the interface thereby slightly lowering the traction coefficient from dry conditions. The amount of lubricant, it's viscosity and the load all alter the lubrication regime at the interface. Lower viscosity fluids such as water are more easily squeezed out than higher viscosity fluids such as oil or semi-solids such as grease [27]. Small amounts of water present on a high roughness surface results in a boundary lubrication regime whereby asperities still interact with one another due to the insufficient lubricant film layer. Higher loads may act to reduce the amount of lubricant further by physically squeezing the water from the interface. Higher loads may have also increased the levels of wear at the interface and this could have caused the friction increase at higher cycles (see Figure 16). Grease lubricated the interface well thereby lowering the traction coefficient considerably providing a smooth run-in for rough surfaces. As the surfaces became smoother (see Figure 11) during grease tests the likelihood of full separation increased contributing to the friction reduction, these results are in agreement with the twin-disc tests conducted by Lewis et al. whereby grease was less effective at higher roughness' [30]. Small amounts of wear were incurred on both the dry and water tests. Dry friction values are in the same range as those seen in twin disc testing using a ground rail surface [31].

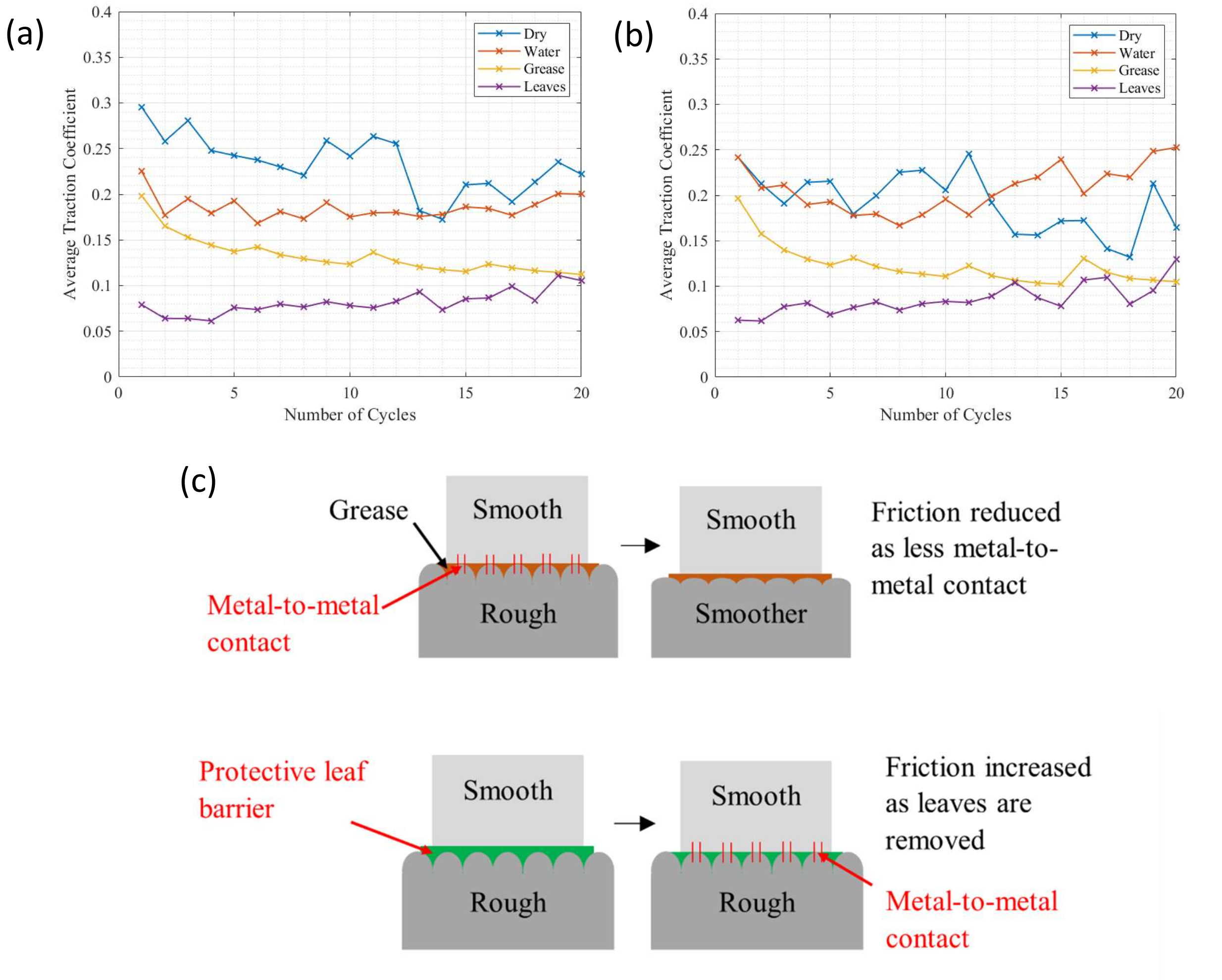

Figure 15. HIR 3BL tests traction coefficient evolution: (a) 600 MPa; (b) 900 MPa and (c) associated mechanism schematics

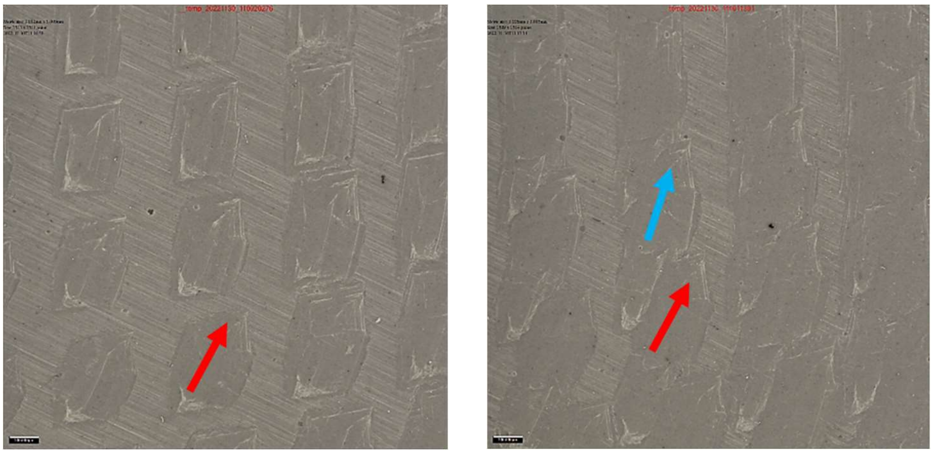

Figure 16. HIR water test lower specimen surfaces showing ploughing (during the first cycle red arrow and the second cycle blue arrow): (a) cycle 1 and (b) cycle 2

4.2.2 Friction - Low Initial Roughness (LIR)

Figure 17 shows the traction coefficient evolution for the LIR tests. The traction coefficients for the LIR tests are generally lower than for the HIR tests, however, this is not always the case. It is expected that for these tests the ploughing force is lower than the for the HIR tests, however, despite these tests having a LIR they are not run-in. They have instead undergone a grinding process to achieve a specific initial roughness that is repeatable. Their initial roughness does, however, represent close to run-in roughness for wheels and rails. As the cycles increase and the surfaces hardness increases, friction resorts to being adhesion force led and stabilises at the interfaces natural tractive state. This can then be altered by the introduction of additional 3BLs or due to drastic topographical changes such as when surfaces incur wear. Wear was incurred on both the dry and water tests, however, visually the water tests incurred more which may have resulted in the higher traction coefficients measured at later cycles see Figure 13. Grease and leaves lubricated the interface well throughout the test which reduced metal-to-metal contact thereby reducing wear. Resultant friction values were similar to the high initial roughness resultant friction values.

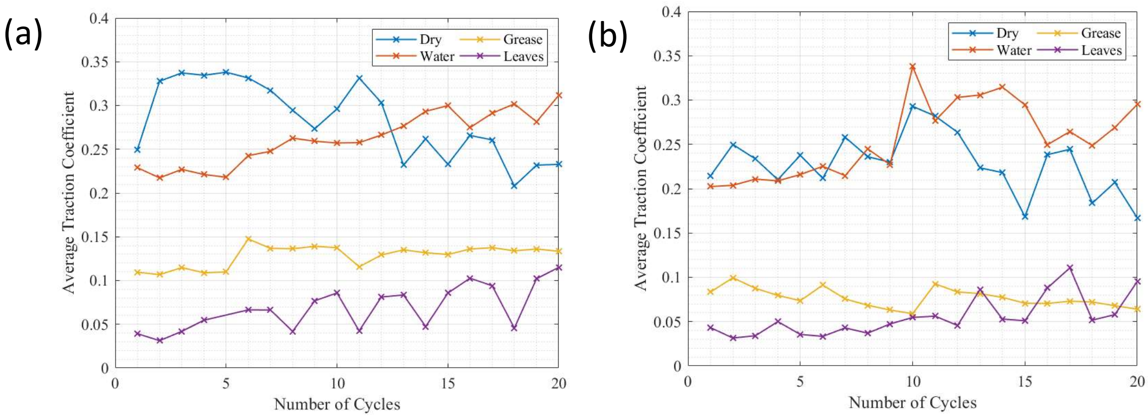

Figure 17. LIR 3BL tests traction coefficient progression: (a) 600 MPa; (b) 900 MPa

Field data form wet and dry rails has been collected using a railhead tribometer [32]. These show the range of dry values to be comparable with those achieved in the HPT tests. The water tests gave lower values than seen for HPT. This was due to the different contact geometry and motion seen in these tests. A similar effect has been seen in slow speed full-scale testing [33].

4.3 Roughness vs Friction

To study the influence roughness has on the traction coefficient only the HIR tests have been compared to the traction coefficients. This has been performed for all 3BLs.

4.3.1 Dry

The average traction coefficient (average from a cycle) appears to drop in a general trend similar to that of the combined roughness, albeit with some variation at points between the beginning and end of the test, during run-in for HIR dry contacts (see Figure 18). As there was no lubrication some adhesion/abrasive wear was observed during tests due to metal-to-metal contact which may have contributed to the erratic traction coefficient progression most notably at higher pressures.

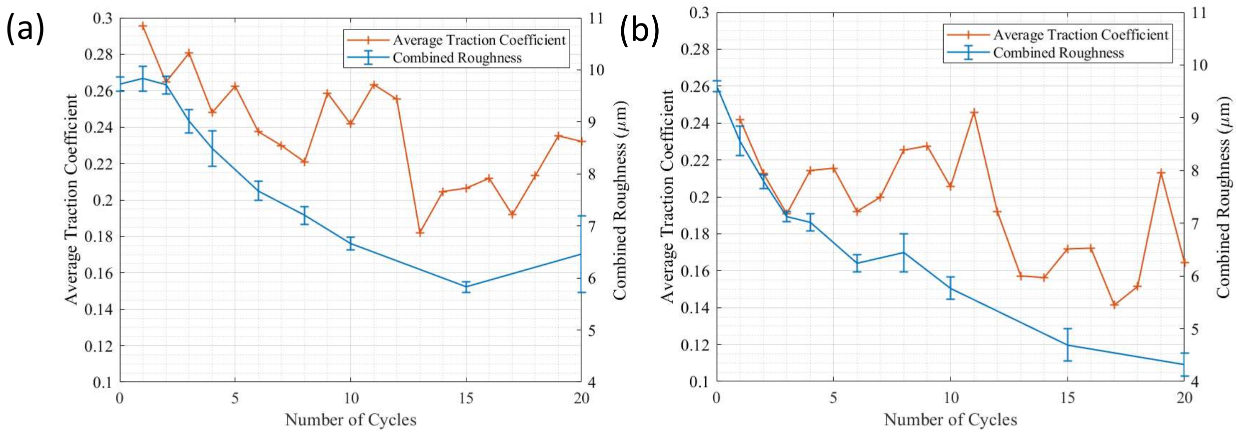

Figure 18. HIR dry tests traction coefficient vs roughness: (a) 600 MPa; (b) 900 MPa

4.3.2 Water

The traction coefficient may be proportional to the combined roughness during run-in for HIR water contacts, however, due to wear, the roughness measurements were not representative of the full contact (see Figure 19). Measured roughness continues to drop for the 900 MPa test, however, the traction coefficient increases. This could be due to the global roughness increasing due to the wear that was incurred that is not represented in the measured roughness (see Figure 19 schematic). Wear mechanisms have been shown to be closely linked to friction and slip [34]. As the roughness reduced, the real contact area may have increased as asperities were 'wiped away' or plastically deformed. This could have resulted in a more adhesion focused wear mechanism. Additionally, as wear occurs the production of wear debris increases the rate of wear, which could act to raise the traction coefficient.

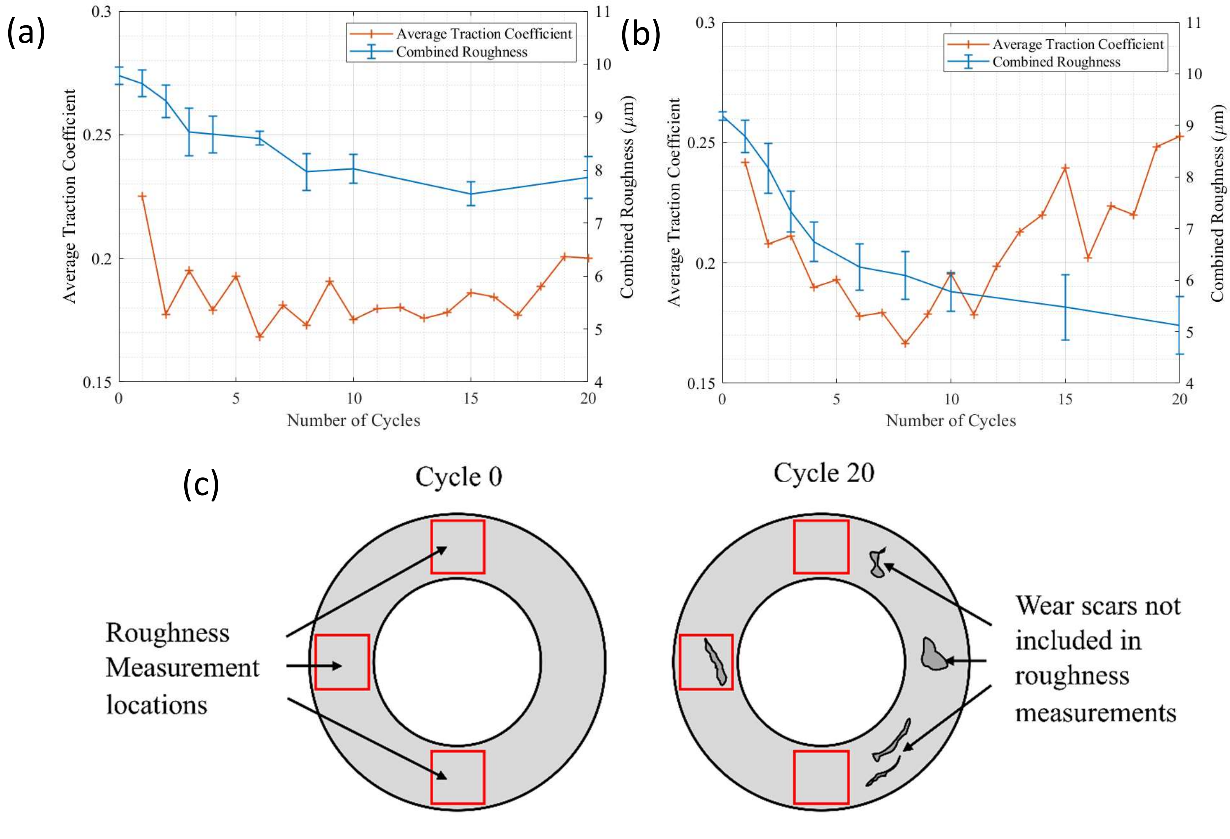

Figure 19. HIR water tests traction coefficient vs roughness: (a) 600 MPa; (b) 900 MPa and (c) associated mechanism schematic

4.3.3 Grease

The traction coefficient decrease was similar for both pressures during the grease tests, however, higher pressures caused both a quicker reduction in roughness and traction coefficient for HIR grease tests (see Figure 20). As expected, grease lubricated the interface well which resulted in little to no wear being incurred on either specimen. This meant that the measured roughness was representative of the global roughness. Higher pressures produced larger roughness reductions which may have contributed to the larger traction coefficient reductions during running in. Grease was applied at various intervals during a test; the relative motion of the two specimens caused this grease to form an established lubricant layer over time. Hill et al. has shown that the disruption of established lubricant layers acts to increase the traction coefficient [35]. Reapplication of the grease was necessary after replication, but this caused sharp (although relatively low) increases in the traction coefficient as seen in Figure 20.

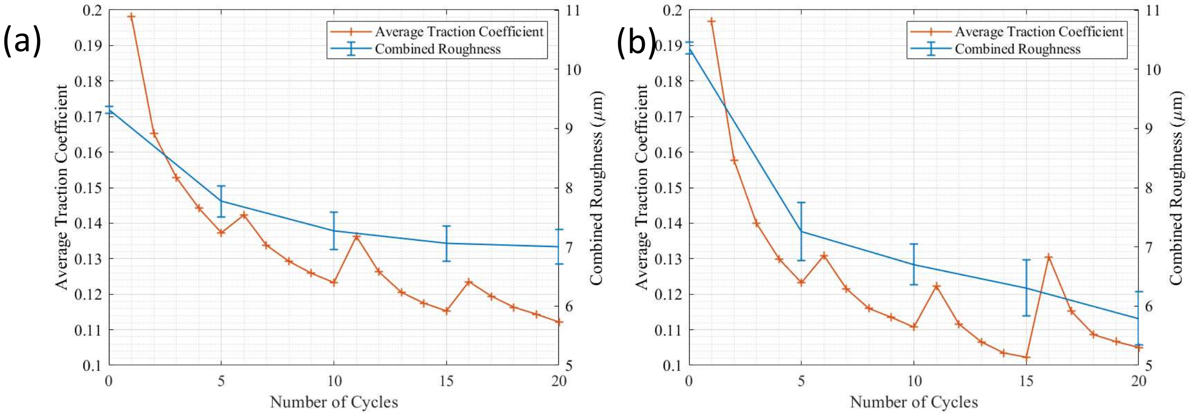

Figure 20. HIR grease tests traction coefficient vs roughness: (a) 600 MPa; (b) 900 MPa

Although much of the grease was expelled from the interface under loading after application, the cleaning and reapplication of grease will have altered the amount of lubricant in the interface and where it is located. This grease must be spread over the surface to form a good lubricant layer which may take numerous cycles. Lubricant film thickness also affects the shear stress between surfaces and for most fluids, viscosity is influenced by the applied pressure and the lubricant temperature. Larger amounts of grease could have acted as a heat sink which could have lowered the interfacial temperature thereby increasing fluid viscosity contributing to the higher tangential forces required to move the surfaces relative to one another. As lubricant temperature was not measured this is only speculation, however the reapplication of grease temporarily increased the measured traction coefficient until the amount/nature of the grease had stabilised.

4.3.4 Leaves

The traction coefficient is not proportional to the combined roughness during run-in for HIR leaf contacts (see Figure 21). Unlike for other 3BLs the traction coefficient increases with increased cycles. The traction coefficient is altered considerably by the presence of leaf layers meaning roughness may no longer be a primary factor.

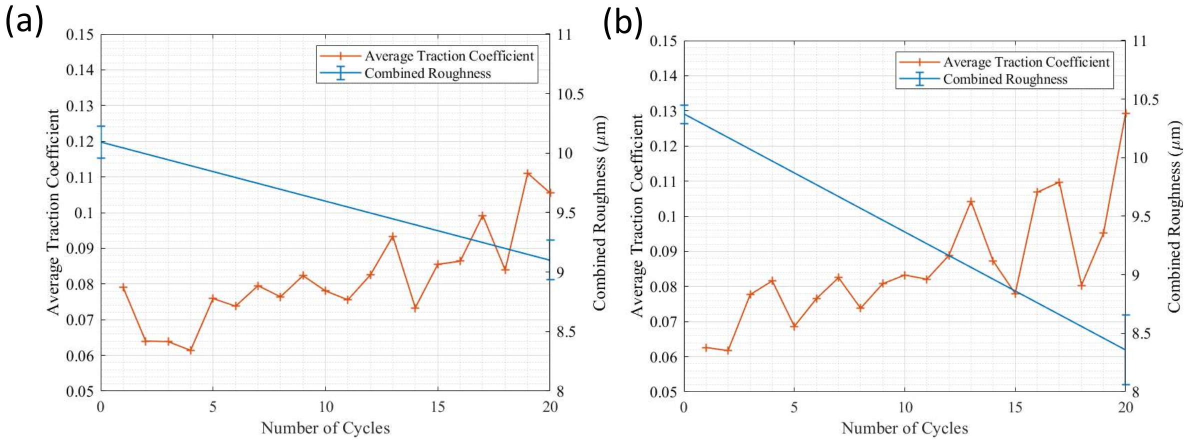

Figure 21. HIR leaf tests traction coefficient vs roughness: (a) 600 MPa; (b) 900 MPa

Higher roughness disrupts the build-up of leaf layers whilst simultaneously slowing the running in process. Whilst it appears that roughness is no longer a primary factor affecting the traction coefficient directly, by disrupting leaf layers that produce ultra-low adhesion conditions (μ<0.1), higher traction coefficients were observed for the leaf tests when the contacts were rougher, see Figure 22.

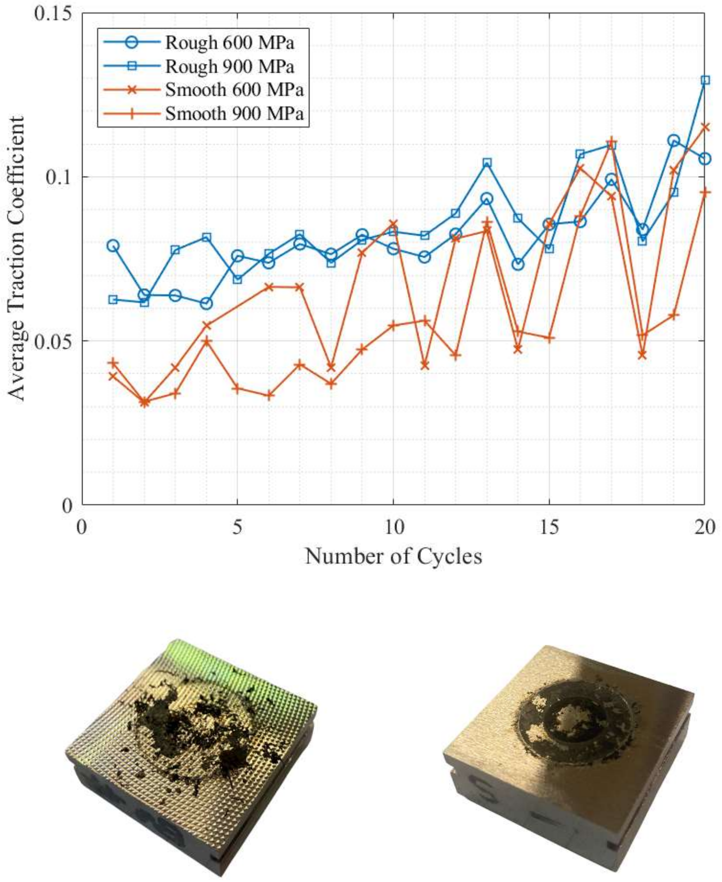

Figure 22. HIR and LIR leaf test layer tests and disruption due to roughness; (a) increasing traction coefficient; (b) HIR surface and (c) LIR surface

5. Conclusions

HPT multi-cycle tests were conducted at two pressures representative of those found in the wheel/rail interface. Two initial roughness' were tested representing freshly ground and run-in rail. Various common third-body layers found on track were applied. Roughness was measured cycle-by-cycle (except for leaf layers) during the tests and the traction coefficient was determined.

Higher pressures resulted in greater roughness reductions for higher initial roughness (ground rail) HIR tests. Dry, water and grease tests produced similar roughness reductions whereas leaf layers slowed roughness progression significantly. Dry and water tests incurred wear due to metal-to-metal contact and slip events. Smooth (low initial roughness (LIR)) tests (run-in rail) visually incurred more wear than the rough tests. Oxides and wear debris were found to be present on the waters tests which may have increased the likelihood of large slip events occurring due to the lubricating effect that these induced. Grease and leaves lubricated the contact reducing the amount of wear for these tests. This resulted in a consistent surface finish. Wheels and rails are able to operate due to a deformed surface layer that has been work hardened. No work hardening was conducted to specimens prior to testing as this would have altered the initial roughness' produced by the machining processes.

Leaves produced ultra-low adhesion conditions ($\mu<0.1$), grease produced low adhesion conditions and water and dry tests produced similar higher adhesion conditions. Traction coefficients generally decreased with decreasing roughness when running in. This was not the case when wear was incurred. For grease tests the surface roughness and traction coefficient were found to be linked. Grease provided a smooth run-in curve with the traction coefficients increasing after grease reapplication. The destruction of the tribofilm during cleaning and replication acted to increase the traction coefficient during the grease tests. Leaves slowed down roughness progression significantly, but it is expected that roughness was not the dominant system component effecting the traction coefficient during these tests as they appeared independent of one another. The presence of leaves was the primary factor in the ultra-low traction coefficients seen. Surprisingly the establishment of the leaf layers during the LIR tests did not reduce the traction coefficient further than the initial measured friction levels, however the disruption of the leaf layers due to higher surface roughness did result in higher traction coefficients.

The new data can be used on its own to help understand roughness evolution post rail grinding and how this may influence friction with and without third-body layers. It can also be used in conjunction with a creep force model to develop creep curves for use as inputs to multi-body simulations to assess train performance in the conditions assessed and also train braking.

Data accessibility

The data will be provided in electronic supplementary material.

Declaration of AI use

We have not used AI-assisted technologies in creating this article.

Authors' contributions

H.S.: formal analysis, investigation, methodology, writing-original draft, writing-review and editing; R.L.: funding acquisition, supervision, writing-review and editing formal analysis, investigation, methodology, writing-original draft, writing-review and editing. W.S.: writing-review and editing. All authors gave final approval for publication and agreed to be held accountable for the work performed therein.

Conflict of interest declaration

We declare we have no competing interests.

Funding

This work was supported by the Engineering and Physical Sciences (UK) Research Council through the iTCDT (grant number EP/L01629X/1) and the Programme Grant "Tribology: The Friction Enigma" (grant number EP/R001766/1) and by the Rail Safety and Standards Board (UK) through project COF-ITR-04 as well.

Acknowledgements

The authors would also like to thank the 'University of Sheffield Institutional Open Access Fund' in cases where this has been used. For the purpose of open access, the author has applied a Creative Commons Attribution (CC BY) license to any Author Accepted Manuscript version arising.

References

[1] Vasic, G., Franklin, F., Kapoor, A., Lucanin, V., 2008, "Laboratory Simulation of Low-Adhesion Leaf Film on Rail Steel", *International Jourrnal of Surface Science and Engineering*, Vol. 2, No. 1-2, pp 84–97, 2008.

[2] Lewis, R., Trummer, G., Six, K., Stow, J., Alturbeh, H., Bryce, B., Shackleton, P., Buckley-Johnstone, L., 2023, "Leaves on the Line: Characterising Leaf based Low Adhesion on Railway Rails", *Tribology International*, Vol. 185, 108529.

[3] Edgley, J., 2018, "Managing low adhesion", *Adhesion Working Group*.

[4] UIC, 2014, "Brakes – Braking Performance", UIC 544-1:6ED 2014.

[5] Lewis, R., Dwyer-Joyce, R.S., Olofsson, U., Pombo, J., Ambrosio, J., Pereira, M., Ariaudo, C., Kuka, N., 2010, "Mapping Railway Wheel Material Wear Mechanisms and Transitions", *Proceedings of the Institution of Mechanical Engineers, Part F: Journal of Rail and Rapid Transit*, Vol. 224, No. 3, pp125–137.

[6] Olofsson, U., Telliskivi, T., 2003, "Wear, plastic deformation and friction of two rail steels: a full-scale test and a laboratory study", *Wear*, Vol. 254, No. 1, pp80–93.

[7] Kumar, S., Yu, G., Witte, A., 1995, "Wheel-Rail Resistance and Energy Consumption Analysis of Cars on Tangent Track with Different Lubrication Strategies", *Proceedings of the 1995 IEEE/ASME Joint Railroad Conference*, Baltimore, USA, 4-6 April, pp129–136.

[8] Shust, W., Elkins, J., 1997, "Wheel forces during flange climb. i. track loading vehicle tests," *Proceedings of the 1997 IEEE/ASME Joint Railroad Conference*, Boston, USA, 18-20 Mar, pp137–147.

[9] Matsumoto, A., Sato, Y., Ohno, H., Tomeoka, M., Matsumoto, K., Kurihara, J., Ogino, T., Tanimoto, M., Kishimoto, Y., Sato, Y., Nakai, T., 2008, "A New Measuring Method of Wheel–Rail Contact Forces and Related Considerations", *Wear*, Vol. 265, No. 9, pp 1518–1525.

[10] Lundmark, J., Höglund, E, Prakash, B., 2006, "Running-in Behaviour of Rail and Wheel Contacting Surfaces", *International Conference on Tribology*, Parma, Italy, 20-22 Sept.

[11] Fukagai, S., Marshall, M.B., Lewis, R., 2022, "Transition of the Friction behaviour and Contact Stiffness due to Repeated High-Pressure Contact and Slip", *Tribology International*, Vol. 170, No. 107487.

[12] Chen, H., Tanimoto, H., 2017, "Experimental Observation of Temperature and Surface Roughness Effects on Wheel/Rail Adhesion in Wet Conditions", *International Journal of Rail Transportation*, Vol. 6, No. 2, pp101-112.

[13] Chang, C.Y., Chen, B., Cai, Y.W., Wang, J.B., 2019, "An Experimental Study of High Speed Wheel-Rail Adhesion Characteristics in Wet Condition on Full Scale Roller Rig", *Wear,* Vol. 440-441, pp440–441.

[14] Evans, M., Skipper, W., Buckley-Johnstone, L., Meierhofer, A., Six, K., Lewis, R., 2021, "The Development of a High Pressure Torsion Test Methodology for Simulating Wheel/Rail Contacts", *Tribology International*, Vol. 156, 106842.

[15] Evans, M.D., Lee, Z.S., Harmon, M., Six, K., Meierhofer, A., Stock, R., Gutsulyak, D.V., Lewis, R., 2023, "Top-of-rail Friction Modifier Performance Assessment: High Pressure Torsion Testing; Creep Force Modelling and Field Validation", *Wear*, Vol. 532-533, 205073.

[16] Skipper, W., Meierhofer, A., Chalisey, A., Six, K., Lewis, R., 2023, "Generation of Sanded Creep Curves using the Extended Creep Force Model with High Pressure Torsion Data", *Wear*, Vol. 542-543, 205278.

[17] Alturbeh, H., Lewis, R., Six, K., Trummer, G., Stow, J., 2020, "Improved Modelling of Trains Braking under Low Adhesion Conditions", *Tribology – Materials, Surfaces and Interfaces*, Vol. 14, No. 3, pp131-141.

[18] Ghidini, A., Diener, M., Gianni, A., Schneider, J., 2012, "Superlos: Innovative Steel by Lucchini RS for High-Speed Wheel Application", *Lucchini RS*, *LRS-Techno*, Vol. 5.

[19] Mädler, K., Zoll, A., Heyder, R., Brehmer, M., 2008, "Rail Materials – Alternatives and Limits", *Zeitschrift fuer Eisenbahnwesen und Verkehrstechnik – Glasers Annalen*, Vol. 132, pp496-503.

[20] Skipper, W.A., Nadimi, S., Chalisey, A., Lewis, R., 2019, "Particle Characterisation of Rail Sands for Understanding Tribological Behaviour", *Wear*, Vol. 432-433, 202960.

[21] Buckley-Johnstone, L.E., Trummer, G., Voltr, P., Meierhofer, A., Six, K., Fletcher, D.I., Lewis, R., 2019, "Assessing the Impact of Small amounts of Water and Iron Oxides on Adhesion in the Wheel/Rail Interface using High Pressure Torsion Testing", *Tribology International*, Vol. 135, pp55-64.

[22] Fukagai, S., Watson, M., Brunskill, H.P., Hunter, A.K., Marshall, M.B., Lewis, R., 2021, "In situ evaluation of contact stiffness in a slip interface with different roughness conditions using ultrasound reflectometry", *Proceedings of the Royal Society. A, Mathematical, Physical, and Engineering sciences*, Vol. 477, No. 2255, pp20210442-20210442.

[23] Six, K., Meierhofer, A., Trummer, G., Bernsteiner, C., Marte, C., Muller, G., Luber, B., Dietmaier, P., Rosenberger, M., 2017, "Plasticity in wheel-rail contact and its implications on vehicle-track interaction", *Proc. Inst. Mech. Eng. Part F J. Rail Rapid Transit*, Vol. 231, No. 5, pp558–569.

[24] Lewis, R., Olofsson, U., 2004, "Mapping Rail Wear Regimes and Transitions", *Wear*, Vol. 257, No. 7-9, pp721-729.

[25] White, B., Nilsson, R., Olofsson, U., Arnall, A., Evans, M., Armitage, T., Fisk, J., Fletcher, D., Lewis, R., 2018, "Effect of the Presence of Moisture at the Wheel–Rail Interface during Dew and Damp Conditions", *Proceedings of the Institution of Mechanical* Engineers, *Part F: Journal of Rail and Rapid Transit*, Vol. 232, pp979-989.

[26] Alicona, 2013, "IF-MeasureSuite, Version 5.1".

[27] Lewis, R., Gallardo, E.A., Hilton, T., Armitage, T., 2009, "Effect of Oil and Water Mixtures on Adhesion in the Wheel/Rail Contact", *Journal of Rail and Rapid Transit, Proceedings of the IMechE Part F*, Vol. 223, pp275-283.

[28] Beagley, T.M., 1976, "The Rheological Properties of Solid Rail Contaminants and their

Effect on Wheel/Rail Adhesion", *Proceedings of the Institution of Mechanical Engineering. Part F*, Vol. 210, No. 4, pp259-266.

[29] Blau, P., 2005, "On the Nature of Running-in", *Tribology International*, Vol. 38, No. 11, pp1007-1012, 2005.

[30] Lewis, S.R., Lewis, R., Evans, G., Buckley-Johnstone, L.E., 2014, "Assessment of Railway Curve Lubricant Performance using a Twin-Disc Tester", *Wear*, Vol. 314, pp 205-215.

[31] Mesaritis, M., Shamsa, M., Cuervo, P., Santa, J., Toro, A., Marshall, M.B., Lewis, R., 2020, "A Laboratory Demonstration of Rail Grinding and Analysis of Running Roughness and Wear", *Wear*, Vol. 456-457, 203379.

[32] White, B., Watson, M., Jaffé, J., Lewis, R., 2025, "A Field Methodology to Assess the Performance of Rail Cleaning, using a New Portable Tribometer", *Journal of Rail and Rapid Transit, Proceedings of the IMechE Part F*, Vol. 239, No. 5, pp421-430.

[33] Lewis, S.R., Fletcher, D.I., Beagles, A., Ishizaka, K., Buckley-Johnstone, L., White, B., Harmon, M., Grigson, C., Brunskill, H., Zhou, L., Kempka, R., Lewis, R., 2018, "A Re-Commissioned Flexible Full-Scale Wheel/Rail Test Facility", *Proceedings of CM2018, 11th International Conference on Contact Mechanics and Wear of Rail/Wheel Systems*, Delft, The Netherlands, 24-26 September 2018.

[34] Lewis, R., Dwyer-Joyce, R.S., 2004, "Wear Mechanisms and Transitions in Railway Wheel Steels," *Proceedings of the Institution of Mechanical Engineering. Part J, Journal of Engineering Tribology*, Vol. 218, No. 6, pp467-478.

[35] Hill, D., Holliman, P.J., McGettrick, J., Appelman, M., Chatterjee, P., Watson, T.M., Worsley, D., 2018, "Study of the Tribological Properties and Ageing of Alkyphosphonic Acid Films on Galvanized Steel," *Tribology International*, Vol. 119, pp337–344.